The Astrophysical Journal, 990:11 (7pp), 2025 September 1 https://doi.org/10.3847/1538-4357/adf746

Unraveling the Role of Neutrino Processes on the Astrophysical Production of ^{94}Mo

N. Song[1], Z. H. Li[1,2,3], G. X. Li[1], Z. C. Gao[1], and Y. F. Niu[4,5]
[1] China Institute of Atomic Energy, Beijing 102413, People's Republic of China; songnanmd@163.com, zhliciae@163.com
[2] School of Nuclear Science and Technology, University of Chinese Academy of Science, Beijing 101408, People's Republic of China
[3] Jinping Deep Underground Frontier Science and Dark Matter Key Laboratory of Sichuan Province, Liangshan 615000, People's Republic of China
[4] School of Nuclear Science and Technology, Lanzhou University, Lanzhou 730000, People's Republic of China
[5] Frontiers Science Center for Rare isotope, Lanzhou University, Lanzhou 730000, People's Republic of China
Received 2025 February 15; revised 2025 July 7; accepted 2025 July 31; published 2025 August 22

Abstract

The enigmatic origin of the proton-rich nuclei ^{92}Mo and ^{94}Mo in the solar system remains one of the most intriguing mysteries in astrophysics, with the definitive production site yet to be identified. Although mechanisms such as the proton-capture reactions, photonuclear reactions, and neutrino processes have been proposed, the underproduction of ^{94}Mo persists as a puzzle. In this study, we investigate the production of ^{94}Mo through neutrino-induced processes during core-collapse supernova explosions. By calculating the cross sections of the charged-current reactions ^{94}Zr $(\nu_e, e^-)^{94}$Nb and ^{95}Mo $(\nu_e, e^-\mathrm{p})^{94}$Mo, as well as the neutral-current reactions ^{95}Mo $(\nu, \nu'\mathrm{n})^{94}$Mo, based on supernova explosion models, we explore the contribution of neutrino-nucleus reactions to the abundance of ^{94}Mo. Our results indicate that these neutrino-induced reactions can account for up to 6.8% of the solar system abundance of ^{94}Mo. Additionally, we propose that specific temperatures and proton number densities formed by neutrino shock waves could reproduce the solar system abundance ratio of ^{94}Mo to ^{92}Mo. This work provides a new perspective on understanding the origin of *p*-process nuclei in the solar system and establishes a significant theoretical foundation for future research endeavors.

Unified Astronomy Thesaurus concepts: Core-collapse supernovae (304); Supernova neutrinos (1666); P-process (1195); Solar abundances (1474)

1. Introduction

The synthesis of elements heavier than iron is primarily driven by the rapid neutron capture process (*r*-process) and the slow neutron capture process (*s*-process). However, the *p*-process is recognized as the key pathway for the synthesis of proton-rich isotopes, which cannot be synthesized via the *s*-process or *r*-process (M. Arnould & S. Goriely 2003). The 35 isotopes on the proton-rich side of the nuclide chart, ranging from ^{74}Se to ^{196}Hg, have abundances approximately 2 orders of magnitude lower than those produced by the *s*-process and *r*-process. Notably, most p-nuclei are approximately 2 orders of magnitude less abundant than other stable isotopes in the same isotope chain, except for the isotopes ^{92,94}Mo and ^{96,98}Ru (M. Arnould & S. Goriely 2003). Their synthesis in stars remains a major unsolved problem in nuclear astrophysics, as current models underproduce their abundances by several orders of magnitude (K. Göbel et al. 2015). Initially, it was believed that proton capture could account for stable nuclei that were bypassed by neutron capture processes and shielded from β-decay. However, subsequent studies on *p*-process nucleosynthesis in stellar environments revealed that the required densities and temperatures are challenging to achieve, particularly for the lightest isotopes of molybdenum and ruthenium (E. M. Burbidge et al. 1957). The currently favored site for the *p*-process is the explosively burning O/Ne layers in core-collapse Type II supernova, where temperatures of $T \sim 2$–3 GK are maintained for approximately 1 s at densities of $\rho = 10^6\ \mathrm{g\,cm^{-3}}$ (T. Sauter & F. Käppeler 1997). This *p*-process in Type II supernova, driven by photodisintegration of heavy seeds, cannot account for the relatively high abundances of ^{92}Mo, ^{94}Mo, ^{96}Ru, and ^{98}Ru (T. Sauter & F. Käppeler 1997). To date, the origin of p-nuclei between $A = 92$ and 126, particularly ^{92}Mo and ^{94}Mo, remains one of the great mysteries in nuclear astrophysics (J. L. Fisker et al. 2008).

The *p*-process production pathways primarily include proton capture, photonuclear reactions, and neutrino processes (ν-process). During the early stages of the core-collapse supernova explosion, the proto-neutron star emits an immense flux of high-energy neutrinos that penetrate the outer layers of the star and trigger nuclear reactions in surrounding nuclei, a process known as the neutrino process. Despite the relatively small interaction cross section of neutrinos with nuclei, the neutrino flux released during supernova explosion is extremely large, making this process become significant source for the production of light and heavy nuclei, rare isotopes, and proton-rich nuclei (S. Woosley et al. 1990; G. Li & Z. Li 2022; N. Song et al. 2022). Investigating the contribution of the neutrino process to the abundance of ^{94}Mo is crucial for understanding the production mechanism of this isotope and for shedding light on the origins of *p*-process nuclei.

In 1995, M. Rayet et al. (1995) conducted calculations to determine the *p*-process yields from core-collapse Type II supernova of solar metallicity stars with masses spanning from $13M_\odot < M < 25M_\odot$. Using comprehensive presupernova and explosion models, they concluded that the production of molybdenum isotopes through the *p*-process was insufficient within the examined mass range. Subsequently, in 2008, J. L. Fisker et al. (2008) investigated the influence of precise measurements of the ^{93}Rh proton separation energy on the synthesis of light molybdenum isotopes in proton-rich ejecta from Type II supernova. They demonstrated that under conditions derived from recent two-dimensional supernova simulations, the

solar ratio of ^{92}Mo to ^{94}Mo could not be reproduced, suggesting that proton-rich winds from Type II supernova may not be the exclusive source for the production of these isotopes. In 2010, F.-K. Thielemann et al. (2010) highlighted the significant sensitivity of the γ-process pathway to uncertainties in reaction rates. They demonstrated that in calculations, even with updated reaction rate data, light p-nuclei remained underproduced in stars with masses (10–25) $M_{\odot}$. Although hydrodynamical simulations show that the conditions in the wind are not extreme enough for an *r*-process up to uranium, neutrino-driven winds following core-collapse supernova are an exciting astrophysical site for the production of heavy elements. These winds may be the site where lighter heavy elements between Sr and Ag are produced, either by the weak *r*-process or by the νp-process (C. Fröhlich et al. 2006). Some studies suggest that ^{92}Mo and ^{94}Mo can be produced under both slightly neutron-rich and proton-rich conditions, with the solar system abundance ratio of the two p-nuclei achievable within neutron-rich conditions for low entropies (J. Bliss & A. Arcones 2015). However, other research indicates that proton-rich winds contribute significantly to the solar abundances of ^{92}Mo and ^{94}Mo, while neutron-rich winds contribute negligibly (J. Bliss et al. 2018). Furthermore, the possibility of reproducing the solar ratio of ^{92}Mo to ^{94}Mo within the high-entropy wind model of core-collapse supernovae has been discussed (K.-L. Kratz et al. 2019; W. Akram et al. 2020). Despite the varying conclusions from existing studies, the underproduction of ^{94}Mo persists. Therefore, our objective is to conduct further theoretical calculations using the neutrino-process to better understand the solar system abundance of ^{94}Mo and to explore the origin of *p*-process nuclei.

In this work, we focus on investigating the abundance of ^{94}Mo produced in neutrino processes. We begin by employing the nuclear gross theory of beta decay (GTBD), considering different Coulomb correction methods, to calculate the cross sections of the ^{94}Zr $(\nu_e, e^-)^{94}$Nb, ^{95}Mo$(\nu_e, e^-\mathrm{p})^{94}$Mo, and ^{95}Mo$(\nu, \nu'\mathrm{n})^{94}$Mo reactions. ^{94}Nb is an unstable isotope that decays to ^{94}Mo via β^- decay with a 100% branching ratio. Next, based on the neutrino spectrum from supernova, we derive the spectrum-weighted cross sections for these reactions. Taking into account the evolution of the neutrino flux and shell temperature, as well as the impact of photodisintegration reactions, we analyze the variation of the ^{94}Mo/^{94}Zr abundance ratio with initial radius, and assess the contributions of the aforementioned reactions to the solar abundance of ^{94}Mo. Finally, we evaluate the specific conditions under which the ^{94}Mo/^{92}Mo can be replicated in the extreme environment characterized by the high temperatures and high proton densities, induced by supernova neutrinos.

2. The Neutrino-nucleus Cross Section

The GTBD model is essentially a parametric model that attempts to combine single-particle dynamics and statistical arguments in a phenomenological way, while also taking into account pairing correlations and shell effects. The cross section of the neutrino-nucleus reaction is primarily determined by the incident energy of the neutrinos, the momentum distribution of the emitted electrons, and the transition matrix elements between the initial and final states of the system. The expression is given by (R. Ferreira et al. 2014; C. A. Barbero et al. 2020)

$$\sigma_{\mathrm{cc}}(E_\nu) = \frac{G_F^2}{\pi}\int_0^{E_\nu - m_e} E_e P_e F_c \times [g_V^2\,|M_F(E)|^2 + g_A^2\,|M_{GT}(E)|^2]\,dE, \quad (1)$$

where $G_F = 1.166 \times 10^{-11}$ MeV^{-2} is the Fermi weak coupling constant. The energy E_{e} and momentum P_{e} of the emitted electrons are represented by $E_e = E_{\nu_e} - E$, $P_e = \sqrt{E_e^2 - m_e^2}$, respectively. E represents the transition energy from the ground state of the parent nucleus to a certain resonant state of the daughter nucleus, and E_ν represents the energy of the incident neutrino. The Coulomb correction factor F_c for the electrons and nuclei interactions can be determined using either the Fermi function (D. Wilkinson & B. Macefield 1974) or the modified effective momentum approximation (MEMA; J. Engel 1998). Since the Fermi function method overestimates Coulomb corrections at high lepton energies and the MEMA method at low energies, the smaller value between the two is typically selected for a more accurate and conservative estimate of the Coulomb effects (J. Engel 1998; C. Volpe et al. 2000; E. Kolbe et al. 2003). The Fermi function $F_{\mathrm{Fermi}}(Z_f, E_e)$, which accounts for the Coulomb correction between electrons and nuclei, is given by

$$F_{\mathrm{Fermi}}(Z_f, E_e) = 2(1+\gamma)(2PR)^{2(\gamma-1)} \times e^{\pi y}\left|\frac{\Gamma(\gamma + iy)}{\Gamma(2\gamma+1)}\right|^2, \quad (2)$$

where $\gamma = [1 - (\alpha Z_f)^2]^{1/2}$, $y = \alpha Z_f E_e/P_e$, and Z_f is the number of protons in the daughter nucleus. $R = 1.2A^{1/3}$ denotes the radius of the daughter nucleus. $\alpha = 1/137$ is the fine structure constant.

In the MEMA approximation, an effective momentum $P_{\mathrm{eff}} = \sqrt{E_{\mathrm{eff}}^2 - m_e^2}$ is utilized, where $E_{\mathrm{eff}} = E_e - V_C(0)$, $V_C(0) = -3Z_f\alpha/2R$ represents the Coulomb potential at the origin. The corresponding correction factor F_{MEMA} is given by $F_{\mathrm{MEMA}} = E_{\mathrm{eff}}P_{\mathrm{eff}}/E_eP_e$ (C. Volpe et al. 2000).

The effective interaction constants of vector and axial-vector are represented by $g_V = g_A = 1$. $|M_F(E)|^2$ and $|M_{GT}(E)|^2$ represent the matrix elements of the Fermi (F) and Gamow–Teller (GT) transitions, respectively. For detailed computational equations, refer to reference N. Song et al. (2025) and R. Ferreira et al. (2014).

Neutrino scattering plays a fundamental role in the core-collapse evolution of a massive star, leading to supernova explosion. In neutral-current (NC) reactions (neutrino scattering), neutrinos (antineutrinos) interact via the exchange of neutral Z^0 bosons with a nucleus as (V. C. Chasioti et al. 2007)

$$\begin{aligned}\nu + (A, Z) &\rightarrow \nu' + (A, Z)^*\\ \bar{\nu} + (A, Z) &\rightarrow \bar{\nu}' + (A, Z)^*,\end{aligned} \quad (3)$$

where ν ($\bar{\nu}$) denotes neutrinos (antineutrinos) of any flavor. The total neutral current neutrino-nucleus cross section is composed of two parts: one is the shell model, which describes the contribution of GT transitions to the cross section, and the other is the contribution from all other multipoles transitions. The GT contribution to the cross section becomes (A. Juodagalvis et al. 2005)

$$\sigma_{\mathrm{nc}}(E_\nu) = \frac{G_F^2}{\pi}\sum_f E'^2_{\nu,if}\,B_{if}(GT), \quad (4)$$

where $E'_{\nu,i,f}$ is the energy of the scattered neutrino, and $E'_{\nu,i,f} = E_\nu + (E_i - E_f)$, where E_i and E_f are the initial and

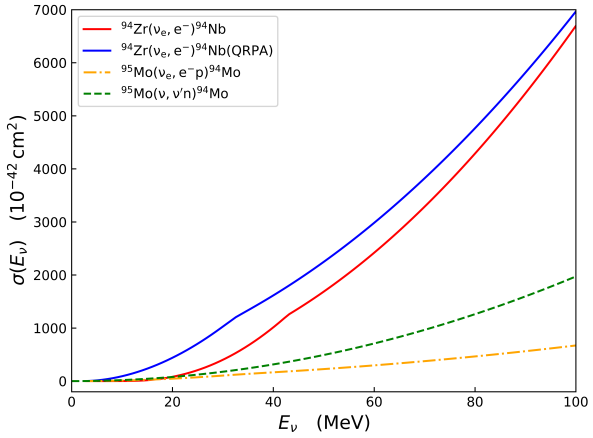

Figure 1. The charged-current neutrino-nucleus cross sections of ^{94}Zr (ν_e, e^-)^{94}Nb and ^{95}Mo(ν_e, e^-p)^{94}Mo reaction, and neutral current cross sections of ^{95}Mo (ν, ν'n)^{94}Mo reaction.

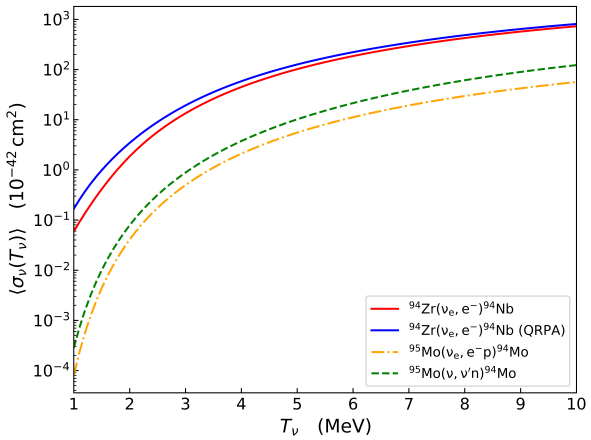

Figure 2. The spectrum-weighted cross sections of ^{94}Zr (ν_e, e^-)^{94}Nb, ^{95}Mo (ν_e, e^-p)^{94}Mo, and ^{95}Mo(ν, ν'n)^{94}Mo reactions.

final nuclear energies, respectively. The GT transition strength between the transition states is calculated using the GTBD model.

We investigated the nuclear synthesis processes responsible for the production of ^{94}Mo, focusing on neutrino-induced reactions involving both charged-current and neutral-current interactions. We specifically applied the GTBD model to calculate the cross section for the charged-current reaction ^{94}Zr (ν_e, e^-)^{94}Nb, where the unstable isotope ^{94}Nb subsequently decays via β^- decay to produce ^{94}Mo. Additionally, we explored the possibility of ^{94}Mo produced via the proton emission of ^{95}Tc after the ^{95}Mo(ν_e, e^-)^{95}Tc reaction. The total cross section is computed with Equation (1). Based on the Hauser–Feshbach theory, we further employed the TALYS model (A. Koning et al. 2021) to calculate the probability of ^{95}Tc emitting a proton once its excitation energy exceeds the proton separation energy, thereby obtaining the cross section for the ^{95}Mo(ν_e, e^-p)^{94}Mo reaction. Simultaneously, the neutrino inelastic scattering reaction ^{95}Mo(ν, ν')^{95}Mo* was investigated as an alternative pathway for ^{94}Mo synthesis, which involves neutron emission. Using Equation (4), the total cross section of the ^{95}Mo(ν, ν')^{95}Mo reaction was determined, along with the neutron emission probability from the excited ^{95}Mo, enabling the calculation of the cross section for the ^{95}Mo(ν, ν'n)^{94}Mo reaction. These three neutrino-induced processes collectively contribute to the production of ^{94}Mo. As shown in Figure 1, the cross sections of the neutrino-induced reactions are dependent on the energy of the incident neutrino. Notably, the ^{94}Zr (ν_e, e^-)^{94}Nb reaction exhibits the largest cross section among the three reactions. The cross section of the ^{94}Zr(ν_e, e^-)^{94}Nb reaction was calculated using the GTBD model and compared with results from the QRPA model, which employs the PC–PK1 interaction (Y. Niu et al. 2013; Z. Wang et al. 2016). The comparison revealed a maximum deviation of less than a factor of 2 between the two models, indicating reasonable agreement within theoretical uncertainties.

The neutrino spectrum-weighted cross section is a critical parameter for determining the yield of ^{94}Mo, as it depends on both the neutrino cross section and the neutrino energy spectrum. It can be expressed as (M.-K. Cheoun et al. 2012; P. C. Divari 2017)

$$\langle\sigma_\nu(T_\nu)\rangle = \int \sigma_\nu(E_\nu) f(E_\nu, T_\nu) dE_\nu, \tag{5}$$

where $f(E_\nu, T_\nu)$ represents the energy spectrum of supernova neutrinos, which is assumed to follow a Fermi–Dirac distribution (P. C. Divari 2017),

$$f(E_\nu, T_\nu) = \frac{0.5546}{T_\nu^3} \frac{E_\nu^2}{\exp(E_\nu/T_\nu) + 1}, \tag{6}$$

where T_ν is the electron neutrino temperature. Previous studies have suggested a high neutrino temperature of $T_\nu = 4$ MeV (S. Woosley et al. 1990; A. Heger et al. 2005). However, A. Sieverding et al. (2018) propose a lower neutrino temperature of $T_\nu = 2.8$ MeV based on spectral data and modern supernova simulations (L. Hüdepohl et al. 2010; G. Martínez-Pinedo et al. 2012, 2014).

Figure 2 presents the spectrum-weighted cross sections of the ^{94}Zr (ν_e, e^-)^{94}Nb, ^{95}Mo(ν_e, e^-p)^{94}Mo, and ^{95}Mo(ν, ν'n)^{94}Mo reactions. These cross sections exhibit an increasing trend with rising neutrino temperatures. The neutrino temperature range of 1–10 MeV, spans the typical temperatures associated with core-collapse supernova explosions. The spectrum-weighted cross section of the ^{94}Zr (ν_e, e^-)^{94}Nb reaction was calculated and compared with the results from the QRPA model. The comparison revealed a maximum deviation of 0.95 times between the two models, indicating reasonable agreement within the theoretical uncertainties. The energy spectrum-weighted cross sections can also be obtained using the semiempirical parametric formula $\langle\sigma_\nu(T_\nu)\rangle_{\rm se} = \exp(a_1 + a_2 T_\nu^{-1} + a_3 T_\nu^{-2} + a_4 T_\nu^{-3} + a_5 T_\nu^{-4} + a_6 \ln(T_\nu))$ (N. Song et al. 2025). The parameters for the energy spectrum-weighted cross sections are provided in Table 1. Notably, the ^{94}Zr (ν_e, e^-)^{94}Nb reaction has the highest spectrum-weighted cross section among the three reactions, indicating its significant role in the production of ^{94}Mo. Based on these findings, we focus on the ^{94}Zr (ν_e, e^-)^{94}Nb reaction as a case to analyze the impact of neutrino-induced processes in core-collapse supernovae on the abundance of ^{94}Mo.

3. Contribution of the ν-process to the Abundance of ^{94}Mo

To estimate the final abundance ratio between ^{94}Mo and ^{94}Zr in the ν-process, we solve the following differential

Table 1
The Fitting Parameters of the Spectrum-weighted Cross Sections of the ^{94}Zr (ν_e, e^-)^{94}Nb, ^{95}Mo(ν_e, e^-p)^{94}Mo, and ^{95}Mo(ν, ν'n)^{94}Mo Reactions

Reaction	a_1	a_2	a_3	a_4	a_5	a_6
^{94}Zr (ν_e, e^-)^{94}Nb	0.83 ± 0.09	7.64 ± 0.36	-21.11 ± 0.73	18.77 ± 0.77	-5.58 ± 0.31	2.32 ± 0.03
^{95}Mo(ν_e, e^-p)^{94}Mo	2.23 ± 0.11	-17.89 ± 0.41	16.52 ± 0.84	-16.01 ± 0.88	5.74 ± 0.35	1.29 ± 0.03
^{95}Mo(ν, ν'n)^{94}Mo	3.73 ± 0.12	-20.38 ± 0.46	19.01 ± 0.93	-15.57 ± 0.98	5.19 ± 0.39	1.28 ± 0.04

equation (N. Song et al. 2022):

$$\frac{dR(T_\nu, t)}{dt} = \phi_\nu(t)\langle\sigma(T_\nu)\rangle - \lambda_\gamma(T(t))R(t), \quad (7)$$

where $R(T_\nu, t)$ denotes the ratio of ^{94}Nb to ^{94}Zr at time t, $\phi_\nu(t)$ represents the neutrino flux, and $\lambda_\gamma(T(t))$ is the reaction rate for the ^{94}Nb$(\gamma, p)^{93}$Zr reaction. The first term on the right-hand side represents the production rate of ^{94}Nb via the ν-process, while the second term corresponds to the destruction rate of ^{94}Nb through photodisintegration.

Assuming ^{94}Zr as the seed nucleus for the production of ^{94}Nb by the ν-process, we consider the initial average radius of the shell is r_0 and the average shock velocity interior to r_0 is $\upsilon_{\rm sh}$. Prior to the arrival of a shock wave, the state of the shell remains almost unchanged. The radius is $r(t < t_0) = r_0$, and the temperature is approximately 1.2 GK, corresponding to the hydrostatic C/Ne shell burning temperature. For a detailed evolution, processes are provided in the reference N. Song et al. (2022). The neutrino flux produced by the explosion process is (S. Woosley et al. 1990)

$$\phi_\nu(t) = \frac{L}{4\pi r^2 n_f \langle E_\nu(T_\nu)\rangle}. \quad (8)$$

At the time $t_0 = r_0/\upsilon_{\rm sh}$, the shock wave arrives, causing the temperature to rise instantaneously to a peak value. Since radiation dominates the internal energy after the shock passage, the explosion energy $E_{\rm expl} \sim 1.2 \times 10^{51}$ erg is related to the peak temperature T_p at a given radius r_0, as

$$T_p = 2.4\left(\frac{E_{\rm expl}}{10^{51}\,{\rm erg}}\right)^{1/4}\left(\frac{r_0}{10^9\,{\rm cm}}\right)^{-3/4}{\rm GK}. \quad (9)$$

The resulting overpressure drives rapid expansion. The expansion of the shocked mass element is nearly adiabatic, with its temperature decreasing exponentially on the hydrodynamic timescale $\tau_{\rm dyn}$ (S. Woosley et al. 1990; G. Li & Z. Li 2022):

$$T(t) = T_{\rm peak} e^{-(t-t_0)/3\tau_{\rm dyn}}, \quad (10)$$

where $\tau_{\rm dyn} \approx 446\rho^{-1/2}$ s and ρ in units of g cm^{-3} represents the mean density interior to the radius r_0. For simplicity, ρ is fixed to a constant 10^5 g cm^{-3} (G. Li & Z. Li 2022). The shocked material in the star's outer layer expands at a typical constant velocity $\nu_p = 5000$ km s^{-1} in the expansion phase (S. Woosley et al. 1990). So the radius of the expanding shell evolves as follows:

$$r(t > t_0) = r_0 + \nu_p(t - t_0) = r_0[1 + (t - t_0)/\tau_p], \quad (11)$$

where $\tau_p = r_0/\nu_p$, the neutrino flux declines more rapidly, as described by (S. Woosley et al. 1990)

$$\phi_\nu(t) = \frac{E_{\rm total}\tau_\nu^{-1} e^{-t/\tau_\nu}}{4\pi r_0^2 n_f \langle E_\nu(T_\nu)\rangle}[1 + (t - t_0)/\tau_p]^{-2}. \quad (12)$$

With a proton separation energy of only 6.54 MeV, ^{94}Nb is susceptible to destruction via the ^{94}Nb$(\gamma, p)^{93}$Zr reaction at high temperatures. The production of ^{94}Nb is closely tied to photonuclear reactions. The reaction rate, which depends on temperature, is given by

$$\lambda_\gamma(T) = c\int_{6.54}^{\infty} n_\gamma(E_\gamma, T)\sigma(E_\gamma)dE_\gamma, \quad (13)$$

where c is the speed of light, and $n_\gamma(E_\gamma, T)$ represents the number density of photons dependent on energy E_γ and temperature T. $\sigma(E_\gamma)$ denotes the cross section for the ^{94}Nb $(\gamma, p)^{93}$Zr reaction. Figure 3 shows the reaction rate for ^{94}Nb $(\gamma, p)^{93}$Zr, based on data from the JINA REACLIB database (R. H. Cyburt et al. 2010). The figure indicates that the reaction rate is highly dependent on temperature, which results in the rapid destruction of ^{94}Nb at high temperatures. Specifically, below 2.95 GK, the reaction rate drops below 1, allowing ^{94}Nb to survive.

As depicted in Figure 4 (top panel), we have studied the evolution of the shell temperature over time at a shock velocity of $\upsilon_{\rm sh} = 5000$ km s^{-1} for various initial radii. Additionally, Figure 4 (bottom panel) illustrates the variation of the abundance ratio $R(T_\nu, t)$ over time. In the figure, initial radii of $r_0 = 6000$, 8000, 10,000, and 12,000 km are represented by purple, red, green, and blue lines, respectively. The figure shows that a smaller initial radius r_0 correlates with a higher neutrino flux before the shock wave arrives, resulting in a larger abundance ratio. However, this also results in the shock wave arriving earlier, rapidly driving the shell temperature to a higher peak. Owing to the temperature sensitivity of the photodisintegration reaction, most of ^{94}Nb is subsequently consumed. Following the shock wave's arrival, the shell temperature drops, reducing the destruction of ^{94}Nb by the photodisintegration and allowing ^{94}Nb to survive, stabilizing the abundance ratio. At this stage, the neutrino flux decreases significantly, and the lower temperature reduces the effectiveness of photodisintegration reactions. For $r_0 = 6000$ km, the final abundance ratio is 5×10^{-4}. When the initial radius is increased to $r_0 = 8000$ km, the shock wave arrives later, and the peak shell temperature is lower, reducing the destruction of ^{94}Nb by photodisintegration. This results in greater retention of ^{94}Nb and a final abundance ratio of 2.2×10^{-3}. For $r_0 = 10{,}000$ km, the shell temperature is low enough to make the photodisintegration reaction nearly ineffective, preserving most of the produced ^{94}Nb and resulting in a final abundance ratio of 1.8×10^{-3}. For $r_0 = 12{,}000$ km, the significant reduction in neutrino flux directly affects the production of ^{94}Nb, especially since photodisintegration processes are negligible. Consequently, the abundance ratio decreases to 1.4×10^{-3}.

From the first term on the right-hand side of Equation (7), which is directly proportional to the spectrum-weighted cross section $\langle\sigma_\nu(T_\nu)\rangle$, inversely proportional to the neutrino temperature T_ν, with additional terms being proportional to $R(T_\nu, t)$. Given identical parameters, the variation in the

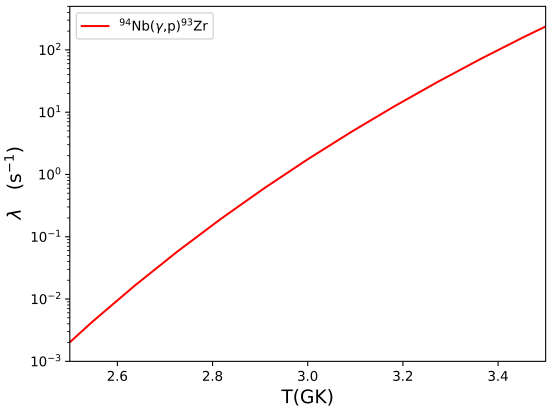

Figure 3. The reaction rate of ^{94}Nb(γ, p)^{93}Zr reaction varies with temperature.

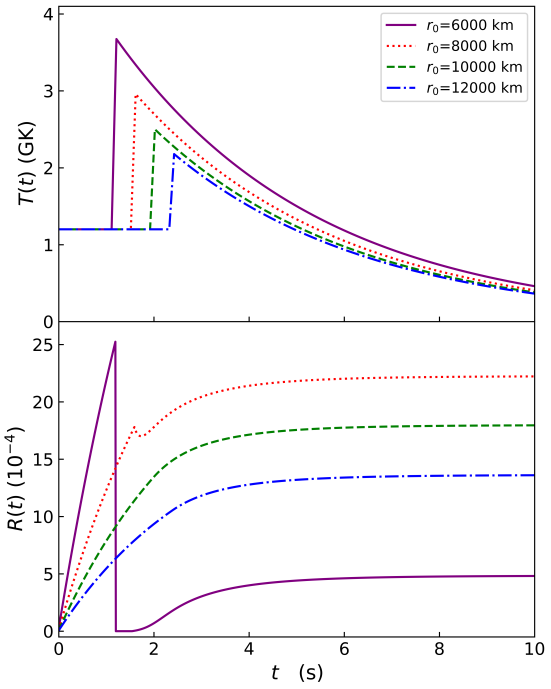

Figure 4. By setting the average shock velocity as $\upsilon_{\rm sh} = 5000\ {\rm km\ s^{-1}}$, the temperatures of the shell (top panel) and the abundance ratios of ^{94}Mo and ^{94}Zr (bottom panel) in the process ^{94}Zr (ν_e, e^-)^{94}Nb vary with time t for different initial average radii of the shell, with neutrino temperatures of 2.8 MeV.

^{94}Mo/^{94}Zr ratio at any given time due to different neutrino temperatures is encapsulated by the factor $\langle\sigma_\nu(T_\nu)\rangle/T_\nu$. Therefore, we choose a specific temperature, such as $T_\nu = 2.8$ MeV, for detailed analysis to determine the optimal average shock wave velocity. To determine the optimal conditions that maximize the ^{94}Mo/^{94}Zr abundance ratio, we calculated its variation over a shock velocity range of $\upsilon_{\rm sh} =$ (5000–20,000) km s^{-1} and initial radii $r_0 =$ (1000–25,000) km, as shown in Figure 5. This analysis is based on the work of S. Woosley et al. (1990), who observed that the star's inner regions expand rapidly at velocities around 20,000 km s^{-1}, while the outer edge of the helium core expands at approximately 5000 km s^{-1}. Our results show that the maximum abundance ratio occurs at 8200 km within the O/Ne shell, closer to the inner shell compared to previously

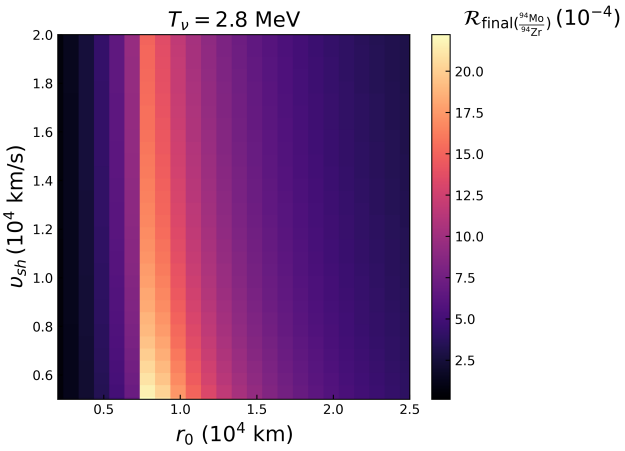

Figure 5. The abundance ratios of ^{94}Mo and ^{94}Zr in the process ^{94}Zr (ν_e, e^-)^{94}Nb vary with the initial radii r_0 for different average shock velocities at neutrino temperature $T_\nu = 2.8$ MeV.

calculated for ^{74}Se (N. Song et al. 2022). Our analysis reveals a decreasing trend in the abundance ratio with increasing shock velocity. The faster shock wave will cause the shell to expand sooner, leading to an earlier rapid decline in the neutrino flux. Conversely, a slower shock wave velocity, arriving later, produces more ^{94}Nb due to a more intense neutrino flux. Though a lower shock velocity enhances ^{94}Nb production, an excessively low velocity would cause the explosion to fail. By analyzing the contribution of neutrino-nucleus reactions to the abundance of ^{94}Mo/^{94}Zr, we find that the maximum abundance ratio is 2.3×10^{-3} when the average shock wave velocity is $\upsilon_{\rm sh} = 5000\ {\rm km\ s^{-1}}$, the initial radius is $r_0 = 8200$ km, and the neutrino temperature is $T_\nu = 2.8$ MeV.

Figure 6 illustrates that the abundance ratios of ^{94}Mo to ^{94}Zr vary with initial radii r_0 for different neutrino temperatures at the optimal average shock wave velocity of $\upsilon_{\rm sh} = 5000\ {\rm km\ s^{-1}}$. The figure shows that the abundance ratio of ^{94}Mo to ^{94}Zr increases gradually with rising neutrino temperature. The solar system abundance ratio of ^{94}Mo to ^{94}Zr is approximately 0.12 (E. Anders & N. Grevesse 1989; K. Lodders 2003). At a neutrino temperature of $T_\nu = 4$ MeV, the maximum abundance ratio of ^{94}Mo to ^{94}Zr is 7.3×10^{-3}, corresponding to 6% of the solar system ratio. Furthermore, the QRPA model was utilized to evaluate the contribution of the ^{94}Zr (ν_e, e^-)^{94}Nb reaction to the ^{94}Mo abundance, yielding a maximum abundance ratio of 8% relative to the solar system value.

Based on the methodologies for calculating abundance ratios, the individual contributions of the charged-current reaction ^{95}Mo(ν_e, e^-p)^{94}Mo and the neutral-current reaction ^{95}Mo (ν, ν'n)^{94}Mo to ^{94}Mo synthesis were evaluated, as summarized in Table 2. Under conditions of $\upsilon_{\rm sh} = 5000\ {\rm km\ s^{-1}}$ and $T_\nu =$ 4 MeV, the reaction ^{95}Mo(ν_e, e^-p)^{94}Mo yields a maximum ^{94}Mo/^{95}Mo abundance ratio of 4×10^{-4}, corresponding to 0.07% of the solar system ratio. Similarly, the reaction ^{95}Mo (ν, ν'n)^{94}Mo produces a maximum ratio of 4.2×10^{-3}, contributing 0.7% to the solar system value. The combined contribution of neutrino-induced reactions to the solar ^{94}Mo abundance attains a maximum of 6.8%. When the QRPA model is applied to calculate the cross section of ^{94}Zr (ν_e, e^-)^{94}Nb, the maximum contribution increases to 8.8% of the solar system ratio. These findings indicate that ^{94}Mo production is not

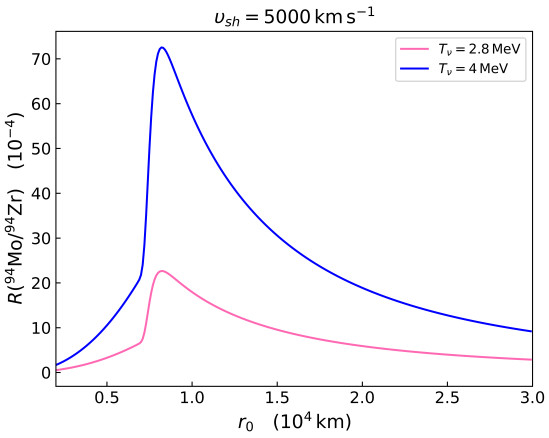

Figure 6. The abundance ratios of ^{94}Mo and ^{94}Zr in the ^{94}Zr $(\nu_e, e^-)^{94}$Nb reaction vary with the initial radii r_0 for different neutrino temperatures, with average shock velocity $\upsilon_{\rm sh} = 5000\ \mathrm{km\ s^{-1}}$.

Table 2
The Contributions of the ^{94}Zr $(\nu_e, e^-)^{94}$Nb, ^{95}Mo$(\nu_e, e^-\mathrm{p})^{94}$Mo, and ^{95}Mo$(\nu, \nu'\mathrm{n})^{94}$Mo Reactions to the Solar System Abundance Ratio of ^{94}Mo at Neutrino Temperatures of 2.8 and 4 MeV

Reaction	Model	The Abundance Ratio	$T_\nu = 2.8$ MeV (%)	$T_\nu = 4$ MeV (%)
^{94}Zr $(\nu_e, e^-)^{94}$Nb	GTBD	R_1	2	6
^{94}Zr $(\nu_e, e^-)^{94}$Nb	QRPA	R_1	2.8	8
^{95}Mo$(\nu, e^-\mathrm{p})^{94}$Mo	GTBD	R_2	0.02	0.07
^{95}Mo$(\nu, \nu'\mathrm{n})^{94}$Mo	GTBD	R_2	0.1	0.7

Note. For convenience, we define two parameters $R_1 = \frac{(^{94}\mathrm{Mo}/^{94}\mathrm{Zr})_{\rm Th}}{(^{94}\mathrm{Mo}/^{94}\mathrm{Zr})_{\rm solar}}$ and $R_2 = \frac{(^{94}\mathrm{Mo}/^{95}\mathrm{Mo})_{\rm Th}}{(^{94}\mathrm{Mo}/^{95}\mathrm{Mo})_{\rm solar}}$, which represent the ratios of the theoretical abundance ratios of ^{94}Mo/^{94}Zr and ^{94}Mo/^{95}Mo to their respective solar system abundance ratios.

exclusively driven by neutrino-nucleus reactions but likely involves additional nuclear processes and reactions.

Given the potential proton-rich environment in supernova neutrino shock waves, we consider conditions with temperatures T ranging from 1 to 3 GK and proton number densities $n_{\rm p} = 10^{27}\,\mathrm{cm^{-3}}$ (C. Fröhlich et al. 2006). At these high temperatures and proton densities, neutrino shock waves may alter the original abundances of nuclei and establish new (p,γ) and (γ,p) equilibria. These equilibria typically occur within the temperature range $T = 1$–2 GK and proton number densities $n_{\rm p} = 10^{26}$–$10^{30}\,\mathrm{cm^{-3}}$ (L. Van Wormer et al. 1994; H. Schatz et al. 1998). The abundance ratio of each nuclide to its two neighboring nuclide in the neutron chain can be determined using the following formula (N. Duy et al. 2021):

$$\frac{Y(N, A+1)}{Y(N, A)} = n_{\rm p}\left(\frac{\hbar^2}{2\pi m_\mu kT}\right)^{3/2} \times \frac{G(N, A+1)}{2G(N, A)} \times \left(\frac{A+1}{A}\right)^{3/2} \times \exp\left[\frac{S_{\rm p}(N, A+1)}{kT}\right], \quad (14)$$

where $Y(N, A)$ represents the abundance of nuclide (N, A), while $Y(N, A+1)$ represents the abundance of nuclide $(N, A+1)$. The variable $n_{\rm p}$ denotes the proton number density, G is the partition function, $S_{\rm p}$ is the proton separation energy of nuclide $(N, A+1)$, k is the Boltzmann constant, and T is the temperature. Given the conditions of temperature and proton number density, the abundance ratio between adjacent nuclides can be calculated.

Once equilibrium is established, the abundances of nuclei are redistributed. As the temperature decreases and equilibrium breaks, some nuclei with higher abundances may transform into ^{94}Mo and ^{92}Mo through β decay. It is known that ^{94}Mo is primarily produced via the β^- decay of ^{94}Nb, with an additional pathway starting from ^{94}Ag along the $A = 94$ chain, decaying to ^{94}Mo with a 100% β^+ decay branch ratio. For ^{92}Mo, the main pathway begins with ^{92}Pd along the $A = 92$ chain, undergoing β^+ decay to ^{92}Mo with a 100% branch ratio. Our calculations indicate that within the temperature range $T = 1.36$–1.77 GK and proton number densities $n_{\rm p} = 3.5 \times 10^{25}$–$2.7 \times 10^{27}\,\mathrm{cm^{-3}}$, the abundance of ^{94}Pd on the $A = 94$ chain is the highest, potentially influencing the abundance of ^{94}Mo. On the $A = 92$ chain, the abundance of ^{92}Ru is the greatest, suggesting that ^{92}Mo may be produced through the β^+ decay of ^{92}Ru. Furthermore, our calculations reveal that at temperatures $T = 1.5$–1.66 GK and proton number densities $n_{\rm p} = 8 \times 10^{25}$–$1 \times 10^{27}\,\mathrm{cm^{-3}}$, the ^{94}Pd/^{92}Ru abundance ratio ranges from 0.6 and 0.64. Consequently, the abundance ratio of ^{94}Mo to ^{92}Mo, produced through the β^+ decay of ^{94}Pd and ^{92}Ru, also falls within this range, consistent with the solar system ^{94}Mo/^{92}Mo abundance ratio. Therefore, we conclude that a proton-rich environment driven by supernova neutrino shock waves, with temperatures between $T = 1.5$ and 1.66 GK and proton number densities $n_{\rm p} = 8 \times 10^{25}$–$1 \times 10^{27}\,\mathrm{cm^{-3}}$, can reproduce the solar system abundance ratio of ^{94}Mo to ^{92}Mo.

4. Conclusion

In this study, we utilized the GTBD model to calculate the cross sections for the charged-current reactions ^{94}Zr $(\nu_e, e^-)^{94}$Nb and ^{95}Mo$(\nu_e, e^-\mathrm{p})^{94}$Mo, as well as the neutral-current neutrino-nucleus reaction ^{95}Mo $(\nu, \nu'\mathrm{n})^{94}$Mo. The spectrum-weighted cross sections were calculated using the neutrino spectrum from supernova explosions. Under supernova explosion models, the variations in shell temperature and neutrino flux before and after the shock arrival were analyzed, and the dependence of abundance ratios on shock velocities and initial radii was systematically explored. Under $\upsilon_{\rm sh} = 5000\,\mathrm{km\,s^{-1}}$ and $T_\nu = 4$ MeV, the maximum ^{94}Mo/^{94}Zr and ^{94}Mo/^{95}Mo abundance ratios correspond to 6% and 0.07% of solar values. Additionally, the reaction ^{95}Mo $(\nu, \nu'\mathrm{n})^{94}$Mo contributes 0.7% to the solar system abundance ratio of ^{94}Mo/^{95}Mo.

We conclude that the contribution of neutrino-induced nuclear reactions to the abundance of ^{94}Mo represents an upper limit of 6.8% of the solar system abundance, indicating that neutrino-nucleus reactions are not the sole pathway for the production of ^{94}Mo. Additionally, regarding the anomaly in the abundance of ^{92}Mo and ^{94}Mo, we find that the solar system abundance ratio between ^{94}Mo and ^{92}Mo can be reproduced in the proton-rich environment with temperatures in the range of 1.5–1.66 GK and proton number densities within $n_{\rm p} = 8 \times 10^{25}$–$1 \times 10^{27}\,\mathrm{cm^{-3}}$, driven by neutrino shock waves. This finding underscores the potential role of supernova neutrino shock waves in the synthesis of p-process nuclei.

Acknowledgments

This work was supported by the National Natural Science Foundation of China under grant Nos. 12475151 and 12405164, and the Continuous-Support Basic Scientific Research Project under grant No. BJ010261223284.

Author Contributions

N.S. undertook the primary work, including research, calculations, and writing; other authors participated in the review and revision of the manuscript.

ORCID iDs

N. Song https://orcid.org/0000-0002-1666-7307
Z. H. Li https://orcid.org/0000-0001-5206-4661
G. X. Li https://orcid.org/0000-0003-4492-8620
Z. C. Gao https://orcid.org/0000-0002-9787-4219
Y. F. Niu https://orcid.org/0000-0003-1029-1887

References

Akram, W., Farouqi, K., Hallmann, O., & Kratz, K.-L. 2020, in EPJ Web of Conf. 227, 23rd Int. Conf. on Computing in High Energy and Nuclear Physics (CHEP 2018), ed. C. Spitaleri et al. (Les Ulis: EDP Sciences), 01009
Anders, E., & Grevesse, N. 1989, GeCoA, 53, 197
Arnould, M., & Goriely, S. 2003, PhR, 384, 1
Barbero, C. A., dos Santos, M. C., & Samana, A. 2020, BrJPh, 50, 331
Bliss, J., & Arcones, A. 2015, arXiv:1509.07621
Bliss, J., Arcones, A., & Qian, Y.-Z. 2018, ApJ, 866, 105
Burbidge, E. M., Burbidge, G. R., Fowler, W. A., & Hoyle, F. 1957, RvMP, 29, 547
Chasioti, V. C., Kosmas, T., & Divari, P. 2007, PrPNP, 59, 481
Cheoun, M.-K., Ha, E., Hayakawa, T., et al. 2012, PhRvC, 85, 065807
Cyburt, R. H., Amthor, A. M., Ferguson, R., et al. 2010, ApJS, 189, 240
Divari, P. C. 2017, Trends in Modern Cosmology (London: InTech)
Duy, N., Uyen, N., & Chae, K. 2021, JKPS, 79, 350
Engel, J. 1998, PhRvC, 57, 2004
Ferreira, R., Dimarco, A., Samana, A. R., & Barbero, C. A. 2014, ApJ, 784, 24
Fisker, J. L., Hoffman, R. D., & Pruet, J. 2008, ApJ, 690, L135
Fröhlich, C., Martinez-Pinedo, G., Liebendörfer, M., et al. 2006, PhRvL, 96, 142502
Göbel, K., Glorius, J., Koloczek, A., et al. 2015, in EPJ Web of Conferences 93, CGS15 - Capture Gamma-Ray Spectroscopy and Related Topics, ed. R. Schwengner & K. Zuber (Les Ulis: EDP Sciences), 03006
Heger, A., Kolbe, E., Haxton, W., et al. 2005, PhLB, 606, 258
Hüdepohl, L., Müller, B., Janka, H.-T., Marek, A., & Raffelt, G. G. 2010, PhRvL, 104, 251101
Juodagalvis, A., Langanke, K., Martínez-Pinedo, G., et al. 2005, NuPhA, 747, 87
Kolbe, E., Langanke, K., Martinez-Pinedo, G., & Vogel, P. 2003, JPhG, 29, 2569
Koning, A., Hilaire, S., & Goriely, S. 2021, Talys-1.96/2.0. simulation of nuclear reactions, User Manual, 2021, 1(2.0), https://nds.iaea.org/talys/
Kratz, K.-L., Akram, W., Farouqi, K., & Hallmann, O. 2019, in AIP Conf. Proc. 2076 (Melville, NY: AIP), 030002
Li, G., & Li, Z. 2022, ApJ, 932, 49
Lodders, K. 2003, ApJ, 591, 1220
Martínez-Pinedo, G., Fischer, T., & Huther, L. 2014, JPhG, 41, 044008
Martínez-Pinedo, G., Fischer, T., Lohs, A., & Huther, L. 2012, PhRvL, 109, 251104
Niu, Y., Niu, Z., Paar, N., et al. 2013, PhRvC, 88, 034308
Rayet, M., Arnould, M., Hashimoto, M., Prantzos, N., & Nomoto, K. 1995, A&A, 298, 517
Sauter, T., & Käppeler, F. 1997, PhRvC, 55, 3127
Schatz, H., Aprahamian, A., Görres, J., et al. 1998, PhR, 294, 167
Sieverding, A., Huther, L., Langanke, K., Martínez-Pinedo, G., & Heger, A. 2018, ApJ, 865, 143
Song, N., Li, Z.-H., Li, G.-X., et al. 2025, ChPhC, 49, 064102
Song, N., Zhang, S., Li, Z., et al. 2022, ApJ, 941, 56
Thielemann, F.-K., Dillmann, I., Farouqi, K., et al. 2010, JPhCS, 202, 012006
Van Wormer, L., Görres, J., Iliadis, C., Wiescher, M., & Thielemann, F.-K. 1994, ApJ, 432, 326
Volpe, C., Auerbach, N., Colo, G., Suzuki, T., & Van Giai, N. 2000, PhRvC, 62, 015501
Wang, Z., Niu, Y., Niu, Z., & Guo, J. 2016, JPhG, 43, 045108
Wilkinson, D., & Macefield, B. 1974, NuPhA, 232, 58
Woosley, S., Hartmann, D., Hoffman, R., & Haxton, W. 1990, ApJ, 356, 272